Swimming with an Image

R. Di Leonardo,[1,2] D. Dell'Arciprete,[2] L. Angelani,[1,2] and V. Iebba[3]
[1]*IPCF-CNR, UOS Roma, Piazzale A. Moro 2, I-00185, Roma, Italy*
[2]*Dipartimento di Fisica, Università di Roma "Sapienza," I-00185, Roma, Italy*
[3]*Dipartimento di Scienze di Sanità Pubblica, Università di Roma "Sapienza," I-00185, Roma, Italy*
(Received 30 July 2010; published 19 January 2011)

The hydrodynamic interactions of a swimming bacterium with a neighboring surface can cause it to swim in circles. For example, when *E. coli* is above a solid surface it had been observed to swim in a clockwise direction. By contrast we observe that, when swimming near a liquid-air interface, the sense of rotation is reversed. We quantitatively account for this through the hydrodynamic interaction of the bacterium with its own mirror image swimming on the opposite side of a perfect-slip boundary. The strength of the coupling is reduced for longer cells, where the torque is spread over a larger length, resulting in longer bacteria swimming in larger circles. We confirm this through precise video measurements of bacterial trajectories and orientations.

DOI: 10.1103/PhysRevLett.106.038101 PACS numbers: 47.63.Gd, 47.15.G−, 68.03.−g, 87.17.Jj

Swimming at low Reynolds number requires a cyclic shape deformation which is not reciprocal, that is not coming back to the original shape retracing the same deformation in reverse order [1]. Bacteria have evolved a clever and simple swimming strategy that consist in spinning a helical flagellum in a continuous rotation. The skewed shape of the flagellum guarantees that a linear translational motion is obtained in response to the torque applied by the flagellar motor [2]. Such a simple swimming strategy does not provide a controlled steering mechanism, but only quite abrupt cell reorientation (tumbles) whenever one or more flagellar motors reverses the sense of rotation and flagella unbundle. The chiral nature of flagella, however, when combined with the presence of a nearby wall, results in a tendency to swim along clockwise circular trajectories above solid surfaces [3,4]. Such a mechanism can be exploited to direct bacterial motions in microchannels [5] or to design microfluidic devices that can sort bacteria according to their motility or size [6]. Hydrodynamic interactions have been shown to be the main factor responsible for clockwise circular trajectories over solid interfaces and also for a tendency of bacteria to remain trapped close to the surface [7]. By changing the hydrodynamic properties of a surface we could think of directing bacterial motions in different directions other than clockwise. A liquid-gas interface provides an almost perfect-slip boundary condition. Free water surfaces are encountered very often in nature, as in the sea surface microlayer, and are highly populated by biological organisms which are collectively referred to as neuston [8]. Moreover, hydrodynamic coupling to different types of interfaces could play an important role in the rectification phenomena recently observed in bacterial ratchet motors [9–11].

In this Letter we demonstrate that *E. coli* bacteria tend to swim along anticlockwise oriented circular trajectories when facing a liquid-air interface. By tracking position, orientation, and length of bacteria we can relate the main trajectories' features to bacterial shape. The radius of curvature of circular trajectories increases almost linearly with the cell body length while the long axis of cell body is always tilted away from the local tangent by an amount that increases for shorter cells. We quantitatively account for this through the hydrodynamic interaction of the bacterium with its own mirror image swimming on the opposite side of a perfect-slip boundary.

E. coli cells (MG1655) were grown overnight at 33 °C in tryptone broth (TB, Difco) containing 1% tryptone and 0.5% NaCl. The saturated culture was then diluted 1:100 (50 μl in 5 ml) into fresh medium and grown at 33 °C until an optical density (600 nm) of 0.4 was reached, corresponding to a middle-log phase. Bacterial cells were harvested from culture media by centrifugation at 2200 rpm for 10 min at room temperature, the pellet was resuspended by gently mixing in prewarmed motility buffer (10 mM potassium phosphate, 0.1 mM Na-EDTA (pH 7.0) 76 mM NaCl, and 0.002% Tween-20 [12]. Bacteria are imaged through the 40× objective of an inverted optical microscope (Nikon TE2000U). The focal plane is located at the bottom free surface of a small solution droplet hanging from a concave glass slide. Trajectories are recorded at 25 frames per second by a digital video recorder. Once a particular bacterium is selected we cut out a small region of interest around it, and after background subtraction and thresholding we extract position and orientation of bacteria from image spatial moments [13]. In particular, cell location is obtained as the image centroid while the orientation of the cell is that of the eigenvector corresponding to the largest eigenvalue of the covariance matrix [Fig. 1(a)]. A sample trajectory is reported in Fig. 1(b). We characterize each trajectory with three parameters: the average speed U, the average curvature radius R, and the mean tilt angle θ between the body axis and the local trajectory tangent

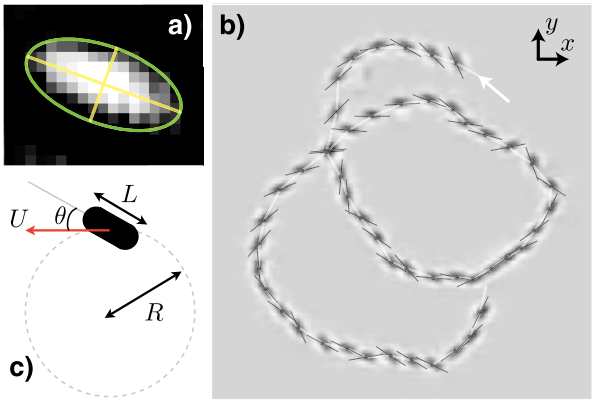

FIG. 1 (color online). (a) Thresholded bacteria image and corresponding covariance ellipsoid. (b) Superposition of frames showing the trajectory of a single cell swimming above a liquid-gas interface. The time interval between frames is 0.16 s. For most of the trajectory the cell axis (black line) is tilted away from the local trajectory tangent. (c) Schematic representation of the main parameters extracted from each trajectory.

[Fig. 1(c)]. In Fig. 2 we report those parameters as a function of cell body length L. Bacterial speeds U have a large variability and an average trend that brings the speed from about 20 to 30 μm/s when the length L goes from 1.5 to 4.5 μm. Such a finding is against what one would predict from the simple hydrodynamic argument that a larger cell body experiences a larger viscous drag and then moves slower when the same flagellar bundle propels it. However, the assumption of an equal flagellar bundle for every cell can be too crude. It is found that the number of flagella can vary [14] and that their average number can increase with increasing body length [15]. Those observations also explain the large fluctuations in speed [Fig. 2(a)]. On the other hand, the trajectory radius R and tilt angle θ are purely geometrical parameters, deriving from velocity ratios and then not depending on the torque applied by the flagellar motor and on viscosity. A variable number of flagella can only affect those two parameters by changing the geometry of the bundle. We will assume in the following that such geometrical variations have negligible effects. As already observed in the proximity of a solid wall, the average radius of curvature R increases almost linearly with L as reported in Fig. 2(b), leading to more straight runs for longer cells. The tilt angle θ of body axis with respect to instantaneous velocity decreases with L, again extrapolating to a linear run for large L. The observed phenomena could be modeled by a boundary element method [16]. A much simpler theoretical approach is based on the composition of resistance matrices, where body and flagellum are treated as two hydrodynamically independent units coupled by rigid constraints [17]. In the case of a solid surface [17] a spherical shape was assumed for the cell body, and the observed increase of the trajectory radius on cell length could only be recovered assuming a gap between cell and wall that increased with body length. We model our swimmer as composed of two rigid

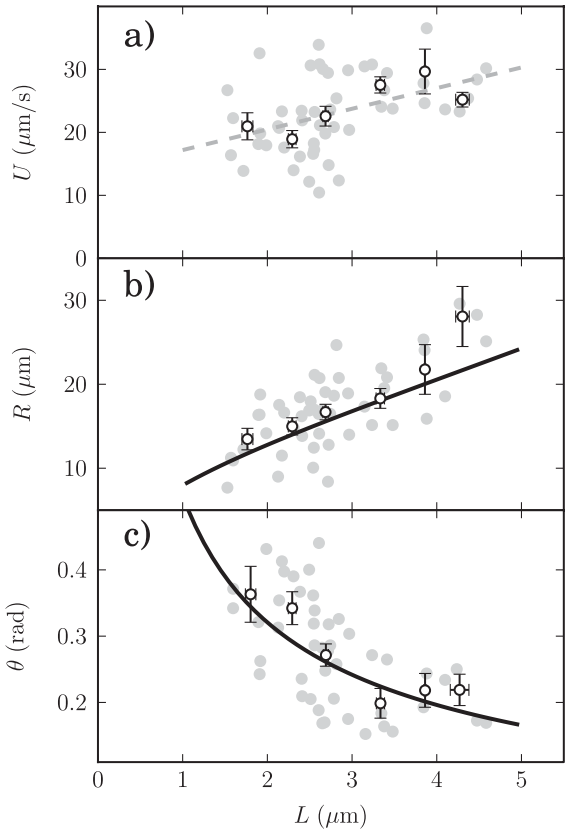

FIG. 2. Cell length (L) dependence of swimming velocity (U), average curvature radius (R) of trajectories, and average tilt angle (θ) of body axis from local trajectory tangent line. Gray circles are raw data, white circles are binned data, and solid black lines represent theoretical predictions when considering a nearby swimming image.

subunits, the cell body (b) and flagellar bundle (f). The two units are rigidly connected but can rotate around a common axis $\hat{\mathbf{x}}$ when a torque is applied by flagellar motors. The motion of each unit can be decomposed into a linear translation of a reference point, usually a center of symmetry, with instantaneous velocity $\mathbf{U}$ and a rotation around the same point with angular velocity $\mathbf{\Omega}$. Linearity of Stokes equations guarantees that the corresponding total force $\mathbf{F}$ and torque $\mathbf{T}$ acting on the unit are linearly related to the components of velocity through the resistance tensors:

$$\begin{aligned} \mathbf{F}^\alpha &= \mathbf{\Gamma}^\alpha \cdot \mathbf{U}^\alpha + \mathbf{C}^\alpha \cdot \mathbf{\Omega}^\alpha, \\ \mathbf{T}^\alpha &= \mathbf{R}^\alpha \cdot \mathbf{\Omega}^\alpha + (\mathbf{C}^\alpha)^T \cdot \mathbf{U}^\alpha, \end{aligned} \tag{1}$$

where the superscript α can be b or f, respectively, for cell body or flagellar bundle. The two symmetric tensors $\mathbf{\Gamma}_\alpha$ and $\mathbf{R}_\alpha$ are, respectively, the translational and rotational drag tensors. The coupling tensor $\mathbf{C}_\alpha$ is nonzero only for skewed bodies, like the helical flagellar bundle, but always vanishes at the center of an orthotropic object like the cell body. Choosing the cell body center as the reference point O, the full dynamical state is described by the linear speed of point O $\mathbf{U}^0 = (u_x^0, u_y^0, u_z^0)$, the axis angular speed $\mathbf{\Omega}_\perp^0 = (0, \omega_y^0, \omega_z^0)$, and the two axial rotational speeds

$\mathbf{\Omega}^b_{||} = (\omega^b_x, 0, 0)$, $\mathbf{\Omega}^f_{||} = (\omega^f_x, 0, 0)$:

$$\mathbf{U}^b = \mathbf{U}^0, \qquad \mathbf{U}^f = \mathbf{U}^0 + \mathbf{\Omega}^0_\perp \times \mathbf{r}^f, \\ \mathbf{\Omega}^\alpha = \mathbf{\Omega}^0_\perp + \mathbf{\Omega}^\alpha_{||}, \tag{2}$$

where $\mathbf{r}^f = (-l/2 - L/2, 0, 0)$. Inserting Eq. (2) into (1) we can obtain expressions for the forces and torques acting on each unit. The total force $\mathbf{F}$ and torque $\mathbf{T}$ acting on the composed object can be readily written in the approximation where we neglect hydrodynamic interactions between the two units and assume that resistance matrices are the same as for the isolated units:

$$\mathbf{F} = \mathbf{F}^b + \mathbf{F}^f, \qquad \mathbf{T} = \mathbf{T}^b + \mathbf{T}^f + \mathbf{r}^f \times \mathbf{F}^f. \tag{3}$$

Once the geometry of the two units is specified, the corresponding drag and coupling tensors are known so that (3) provides six linear relations connecting the components of the total force and torque to the seven variables: u^0_x, u^0_y, u^0_z, ω^0_y, ω^0_z, ω^b_x, ω^f_x. The whole swimmer has to be force free and torque free so that the resistance problem (3) directly provides six equations in seven unknowns which we use, for example, to express the full object dynamical state as a function of the rotational speed of the flagellum. When a bacterium swims in the proximity of a wall, flow fields are furthermore subject to the boundary conditions imposed by the wall. A perfect-slip boundary condition requires a vanishing z component of flow and vanishing z gradients at the interface. This condition can be easily satisfied for a system of point forces by considering the bulk flow produced by adding to each real force its mirror reflection through the interface plane. Swimming close to a free surface is then approximately equivalent to having a specular image bacterium swimming on the opposite side. The physical picture is then that of a bacterium swimming in the flow field produced by its image. Such an image will move with the same speed of the original cell, but the image body and bundle will rotate in opposite direction with respect to the real bacterium. The flow produced by the two rotating units will advect the cell body in the positive y direction and the bundle in the negative y direction, resulting in a rotation of the bacterium in the anticlockwise direction when viewed from above the surface (Fig. 3). Bacteria will then trace circular runs in anticlockwise direction until a tumble event reorients the cell. The flow field produced by the image cell body will also tilt its velocity vector away from the body axis. We will now take into account the hydrodynamic interactions between each unit and its own image separately. Cross correlations, such as that between bundle image and real body, are found to have a negligible effect on the in plane (xy) dynamics and are neglected here. However, they are mainly responsible for hydrodynamic attraction between the whole bacterium and its image and have to be included to reproduce hydrodynamic entrapment to the surface [7]. Hydrodynamic interactions are easily described in a mobility formulation and then get the corrected resistance tensors by inversion.

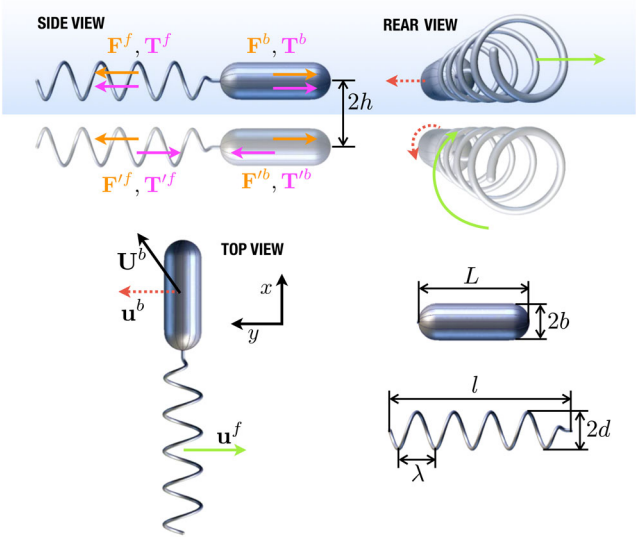

FIG. 3 (color online). Side, rear, and top views of the swimming bacterium and corresponding image bacterium on the opposite side of the interface. Solid green and dotted red arrows in rear and top views represent the flows produced by the rotating images of, respectively, the flagellar bundle and the body.

Each unit will find itself in the flow field produced by its own image. We expand such a flow field about the unit center as a rigid translation $\mathbf{u}$ and a rotation $\boldsymbol{\omega}$:

$$\mathbf{U}^\alpha = \mathbf{M}^\alpha \cdot \mathbf{F}^\alpha + \mathbf{D}^\alpha \cdot \mathbf{T}^\alpha + \mathbf{u}^\alpha, \\ \mathbf{\Omega}^\alpha = \mathbf{K}^\alpha \cdot \mathbf{T}^\alpha + (\mathbf{D}^\alpha)^T \cdot \mathbf{F}^\alpha + \boldsymbol{\omega}^\alpha, \tag{4}$$

where $\mathbf{M}$ and $\mathbf{R}$ are, respectively, the translational and rotational mobility tensors, $\mathbf{D}$ is the coupling tensor in the mobility formulation. Anisotropic bodies also tend to align with the principal axis of strain [18]. In our geometry however, this alignment is automatically fulfilled. The velocity $\mathbf{u}$ will linearly depend on the total force $\mathbf{F}'^\alpha$ and torque $\mathbf{T}'^\alpha$ applied on the image units:

$$\mathbf{u}^\alpha = \mathbf{G}^{uF} \cdot \mathbf{F}'^\alpha + \mathbf{G}^{uT} \cdot \mathbf{T}'^\alpha, \\ \boldsymbol{\omega}^\alpha = \mathbf{G}^{\omega T} \cdot \mathbf{T}'^\alpha + \mathbf{G}^{\omega F} \cdot \mathbf{F}'^\alpha. \tag{5}$$

If we call $\boldsymbol{\sigma} = \mathrm{diag}(1, 1, -1)$ the mirror reflection operator, we have $\mathbf{F}'^\alpha = \boldsymbol{\sigma} \cdot \mathbf{F}^\alpha$ and $\mathbf{T}'^\alpha = -\boldsymbol{\sigma} \cdot \mathbf{T}^\alpha$. The minus sign in the second equation comes from the fact that torques are pseudovectors. Substituting in (5) and the result in (4) we obtain the two units mobilities corrected for the presence of the corresponding images:

$$\overline{\mathbf{M}^\alpha} = \mathbf{M}^\alpha + \mathbf{G}^{uF} \cdot \boldsymbol{\sigma}, \qquad \overline{\mathbf{K}^\alpha} = \mathbf{K}^\alpha - \mathbf{G}^{\omega T} \cdot \boldsymbol{\sigma}, \\ \overline{\mathbf{D}^\alpha} = \mathbf{D}^\alpha - \mathbf{G}^{uT} \cdot \boldsymbol{\sigma}. \tag{6}$$

The corresponding resistance matrices can be obtained by inversion of the block matrix:

$$\begin{pmatrix} \overline{\mathbf{\Gamma}^\alpha} & \overline{\mathbf{C}^\alpha} \\ \overline{\mathbf{C}^{\alpha T}} & \overline{\mathbf{R}^\alpha} \end{pmatrix} = \begin{pmatrix} \overline{\mathbf{M}^\alpha} & \overline{\mathbf{D}^\alpha} \\ \overline{\mathbf{D}^{\alpha T}} & \overline{\mathbf{K}^\alpha} \end{pmatrix}^{-1}. \tag{7}$$

Once the resistance matrices are obtained we can calculate the total force and torque on the composed object and solve dynamics by setting the force and torque to zero. We approximate the cell body as a prolate ellipsoid whose mobility tensors are known analytically [19]. The flagellar bundle is modeled as a helical slender body of thickness $2r_0 = 20$ nm, length $l = 7.5$ μm, pitch $\lambda = 2.3$ μm, and radius $d = 0.2$ μm [14]. The corresponding resistance matrix is calculated analytically with resistive force theory (see supplementary material [20]). As we already qualitatively described, the tendency to swim in anticlockwise circular trajectories has to be mainly attributed to the y component of the flows produced by image bodies. The largest contribution to that component comes from the x component of the image torques. If we remind the reader that both units are elongated bodies with the major axis aligned parallel to a close interface, we soon realize that a point rotlet would be a too crude an approximation for the flow propagator $\mathbf{G}^{uT}$. Therefore we choose to represent the flow produced by such image torques as the near field flow produced by a cylinder of length ℓ^α that is [21]

$$\mathbf{G}_{yx}^{uT} = \frac{1}{8\pi\mu h\ell^\alpha}. \tag{8}$$

That is the most crucial assumption to reproduce experimental data. Once that component is set, practically any reasonable choice for the remaining components of flow propagators has only a tiny effect on the observed quantities. Most of those components vanish for symmetry reasons, while those applied to y and z components of forces and torques will in general have a small effect compared to those applied to the much bigger x components. A very simple choice is that of using point propagators for all other nonzero components. With that choice we are able to get a very good quantitative agreement with experimental data as shown by solid black lines in Figs. 2(b) and 2(c). The most sensitive parameter is also the least accessible one, which is the gap between body and interface $(h - b)$. Gap estimates for solid walls have been reported to be below 100 nm [22], although more recent numerical simulations seem to suggest values as large as a few hundreds of nanometers [23]. We find the best agreement when using a gap value of 350 nm. A large gap value could also compensate for the assumption of a perfect-slip boundary condition or the possible reduction of image flows due to a layer of increased viscosity.

In conclusion, we have shown that *E. coli* bacteria swimming in the proximity of a free liquid interface tend to follow anticlockwise circular trajectories. Such behavior, already hypothesized in [17], can be quantitatively described through the hydrodynamic interaction of the real bacterium with its mirror image swimming on the opposite side of the interface. In this model the cell body rotation is mainly attributed to the advection of the real bacterium by the flows produced by the two counterspinning images. In particular, the flow due to the spinning of the cell body decreases as the inverse of cell body length. As a consequence of this reduced flow, both the curvature and tilt of the body axis increase for shorter cells leading to a strong size dependent deflection mechanism. It would be interesting to check whether such a behavior is maintained when swimming on superhydrophobic surfaces where most of the surface area is again a liquid-gas interface. In this case, one could think of new strategies to sort and direct bacterial motions in microchannels by modulating the slip length on the channel walls.

This work was supported by IIT-SEED BACTMOBIL project and MIUR-FIRB project RBFR08WDBE.

[1] E. Purcell, Am. J. Phys. **45**, 3 (1977).
[2] H. C. Berg, *E. coli in Motion* (Springer-Verlag, New York, 2004).
[3] H. C. Berg and L. Turner, Biophys. J. **58**, 919 (1990).
[4] P. Frymier, R. Ford, H. C. Berg, and P. Cummings, Proc. Natl. Acad. Sci. U.S.A. **92**, 6195 (1995).
[5] W. DiLuzio *et al.*, Nature (London) **435**, 1271 (2005).
[6] S. Hulme, W. DiLuzio, S. Shevkoplyas, and L. Turner, Lab Chip **8**, 1888 (2008).
[7] A. P. Berke, L. Turner, H. C. Berg, and E. Lauga, Phys. Rev. Lett. **101**, 038102 (2008).
[8] M. I. Gladyshev, *Biophysics of the Surface Microlayer of Aquatic Ecosystems* (IWA Publishing, London, 2002).
[9] L. Angelani, R. Di Leonardo, and G. Ruocco, Phys. Rev. Lett. **102**, 048104 (2009).
[10] R. Di Leonardo *et al.*, Proc. Natl. Acad. Sci. U.S.A. **107**, 9541 (2010).
[11] A. Sokolov, M. M. Apodaca, B. A. Grzybowski, and I. S. Aranson, Proc. Natl. Acad. Sci. U.S.A. **107**, 969 (2009).
[12] J. Adler and B. Templeton, J. Gen. Microbiol. **46**, 175 (1967).
[13] W. K. Pratt, *Digital Image Processing* (John Wiley & Sons, New York, 2001).
[14] L. Turner, W. Ryu, and H. C. Berg, J. Bacteriol. **182**, 2793 (2000).
[15] S. Chattopadhyay, R. Moldovan, C. Yeung, and X. L. Wu, Proc. Natl. Acad. Sci. U.S.A. **103**, 13 712 (2006).
[16] M. Ramia, D. Tullock, and N. Phan-Thien, Biophys. J. **65**, 755 (1993).
[17] E. Lauga, W. DiLuzio, G. Whitesides, and H. Stone, Biophys. J. **90**, 400 (2006).
[18] E. Lauga, Rep. Prog. Phys. **72**, 096601 (2009).
[19] S. Kim and S. J. Karrila, *Microhydrodynamics: Principles and Selected Applications* (Dover, New York, 2005).
[20] See supplemental material at http://link.aps.org/supplemental/10.1103/PhysRevLett.106.038101 for an analytical derivation of the helix resistance matrix within resistive force theory.
[21] L. Landau and E. Lifshitz, *Fluid Mechanics* (Pergamon, New York, 1959).
[22] M. Vigeant, R. Ford, M. Wagner, and L. Tamm, Appl. Environ. Microbiol. **68**, 2794 (2002).
[23] D. Giacché, T. Ishikawa, and T. Yamaguchi, Phys. Rev. E **82**, 056309 (2010).